A Numerical Method for Parallel Particle Motions in Gyrokinetic Vlasov Simulations*)

Shinya MAEYAMA, Akihiro ISHIZAWA[1)], Tomo-Hiko WATANABE[1)], Noriyoshi NAKAJIMA[1)], Shunji TSUJI-IIO and Hiroaki TSUTSUI

Tokyo Institute of Technology, 2-12-1 Ookayama, Meguro-ku 152-8550, Japan
[1)]*National Institute for Fusion Science, 322-6 Oroshi-cho, Toki 509-5292, Japan*

(Received 15 December 2010 / Accepted 21 February 2011)

A semi-Lagrangian scheme is applied for the first time to computations of charged particle motions along magnetic field lines, to numerically solve the δf gyrokinetic equations in a flux tube geometry. This new solver adopted in the gyrokinetic Vlasov simulations has an advantage over the conventional Eulerian codes in calculating the parallel dynamics, because semi-Lagrangian schemes are free of the Courant-Friedrichs-Lewy (CFL) condition that restricts the time step size. A study of the accuracy of the parallel motion simulations reveals that numerical errors mainly stem from spatial (not temporal) discretization for realistic values of the grid spacing and time step, and it demonstrates the advantage of the semi-Lagrangian scheme. This novel numerical method is successfully applied to linear gyrokinetic simulations of the ion temperature gradient instability, where time steps larger than those restricted by the CFL condition can be employed.

Keywords: gyrokinetic simulation, semi-Lagrangian scheme, symplectic integrator

DOI: 10.1585/pfr.6.2401028

1. Introduction

Gyrokinetic simulations are useful tools for studying turbulent transport in toroidal plasmas. The development of numerical techniques for these simulations has continued to improve their applicability, accuracy, and efficiency. Recently, Pueschel *et al*. discovered that high-$k_\parallel$ numerical oscillations due to the discretization of the field-aligned coordinate cause a numerical problem in flux tube gyrokinetic simulations [1]. The Vlasov simulation codes that solve the gyrokinetic equation as a partial differential equation in the phase space often introduce artificial (hyper) diffusion to suppress the numerical oscillations. To lower the influence of the numerical dissipation on physical results, the grid spacing should be less than the parallel wavelengths: this has expensive computational costs and leads to a time step size that is severely restricted by the Courant-Friedrichs-Lewy (CFL) condition in explicit Eulerian schemes. This is crucial to gyrokinetic simulations of the kinetic ballooning mode in high-β plasmas and micro instabilities in helical systems with many ripples.

In contrast with Eulerian schemes, semi-Lagrangian schemes do not suffer from the CFL condition. The GYSELA code [2] solves the global full-f gyrokinetic equations with a semi-Lagrangian scheme and is applied to the ion-temperature-gradient (ITG)-driven turbulence in tokamak plasmas. To our knowledge, however, there exists no flux tube gyrokinetic code implemented with a semi-Lagrangian scheme.

In this paper, we apply a semi-Lagrangian scheme to the parallel dynamics, described by Poisson brackets for the field-aligned coordinate and the parallel velocity, in a flux tube gyrokinetic Vlasov simulation. The application is made in three steps. First, the spatial accuracy of the semi-Lagrangian scheme is evaluated for the one-dimensional linear advection problem. Second, the parallel particle dynamics in the two-dimensional phase space is tested, where sufficient number of spatial grid points is needed to avoid unphysical fluctuations. It is demonstrated that the semi-Lagrangian scheme with a time splitting method enables us to take large time step sizes even with a fine mesh. Third, linear gyrokinetic simulations of the ITG instability are performed by implementing the semi-Lagrangian scheme in the GKV code [3], which was originally developed as a Eulerian code for simulations of the electrostatic ITG turbulence.

2. Parallel Dynamics in Gyrokinetics

Using the flux tube approximation [4], the linearized gyrokinetic Vlasov equation for the perturbed ion gyrocenter distribution function δf in the electrostatic limit is given by

$$\left(\frac{\partial}{\partial t} + v_\parallel \nabla_\parallel + \mathbf{v}_\mathrm{d}\cdot\nabla - \frac{\mu\nabla_\parallel B}{m_\mathrm{i}}\frac{\partial}{\partial v_\parallel}\right)\delta f = -\frac{eF_\mathrm{M}}{T_\mathrm{i}}\left[v_\parallel\nabla_\parallel + (\mathbf{v}_\mathrm{d}-\mathbf{v}_*)\cdot\nabla\right]\Phi, \quad (1)$$

where B, m_i, e, F_M, T_i, $\mathbf{v}_\mathrm{d}$, and $\mathbf{v}_*$ are the magnetic field

author's e-mail: smaeyama@nr.titech.ac.jp

*) This article is based on the presentation at the 20th International Toki Conference (ITC20).

strength, ion mass, elementary charge, Maxwellian distribution function, ion temperature, magnetic drift velocity, and diamagnetic drift velocity, respectively. The parallel velocity $v_\parallel$ and magnetic moment μ are employed as the velocity space coordinates. The parallel gradient for a large aspect ratio tokamak with concentric circular magnetic surfaces is written as $\nabla_\parallel = (1/qR_0)\partial_z$, where q, R_0, and z are the safety factor, major radius, and field-aligned coordinate, respectively. Periodic boundary conditions are assumed in the perpendicular coordinates x and y. The gyrocenter electrostatic potential Φ is related to the electrostatic potential ϕ by $\Phi_{k_x,k_y} = J_0(k_\perp\rho_\mathrm{i})\phi_{k_x,k_y}$ in the perpendicular wave number space, where J_0, $k_\perp$, and ρ_i are the zeroth-order Bessel function, perpendicular wave number, and ion Larmor radius, respectively. The electrostatic potential is determined by the quasi-neutrality condition with an adiabatic electron response [3].

By neglecting the gyrocenter electrostatic potential and the perpendicular motions (the magnetic and diamagnetic drifts), one can focus on the parallel dynamics in the gyrokinetic Vlasov equation

$$\frac{\partial f}{\partial t} + \{f, K\}_\parallel = 0, \tag{2}$$

where $K = v_\parallel^2/2 + \mu B/m_\mathrm{i}$ is the particle kinetic energy per unit mass and $\{f, g\}_\parallel = \nabla_\parallel f \partial_{v_\parallel} g - \partial_{v_\parallel} f \nabla_\parallel g$ denotes the parallel Poisson brackets. Equation (2) represents the field-aligned advection of f characterized by the parallel particle motions of

$$\frac{\mathrm{d}s}{\mathrm{d}t} = \{s, K\}_\parallel, \tag{3}$$

where $s = (qR_0 z, v_\parallel)$ are the canonical coordinates.

3. Numerical Schemes

3.1 Symplectic integrator and splitting method

The parallel particle motions are characterized by the Poisson brackets with the additive separable Hamiltonian, $K(z, v_\parallel) = T(v_\parallel) + V(z)$, where $T(v_\parallel) = v_\parallel^2/2$ and $V(z) = \mu B(z)/m_\mathrm{i}$ for a fixed μ. Introducing the differential operators $D_T(s) = \{s, T\}_\parallel$ and $D_V(s) = \{s, V\}_\parallel$, the formal solution of Eq. (3) is given by

$$s(t + \Delta t) = \exp\left[\Delta t(D_T + D_V)\right] s(t). \tag{4}$$

We obtain an approximation to Eq. (4) by splitting the time integration as follows:

$$s(t + \Delta t) = \prod_{j=1}^{k} \exp\left(c_j \Delta t D_T\right) \exp\left(d_j \Delta t D_V\right) s(t), \tag{5}$$

which is known as a symplectic integrator consisting of elementary symplectic mappings. The coefficients c_j and d_j can be found in Ref. [5]. This integrator is applied to the mapping of f, which leads to the splitting of the time integration in Vlasov simulations [6].

3.2 Semi-lagrangian scheme

Considering Eq. (2) as an advection equation, the value at $(z, v_\parallel)$ is updated with that at the departure point (ζ, v):

$$f(t + \Delta t, z, v_\parallel) = f(t, \zeta, v). \tag{6}$$

The departure point $(\zeta(\Delta t, z, v_\parallel), v(\Delta t, z, v_\parallel))$ is obtained from the characteristic curves defined by Eq. (3). By means of the splitting method, Eq. (2) can be split into two linear advection problems in z and $v_\parallel$. Then, we can compute the value of f at the departure point from its values on the grid points by using one-dimensional interpolations. Here, three interpolation methods are examined: the cubic Lagrange interpolation (CLI), the cubic Hermite interpolation (CHI), and the quintic interpolation using second derivatives (QI2) [7]. QI2 is given by

$$\begin{aligned} Q_5(\alpha) = {} & \beta^3(1 + 3\alpha + 6\alpha^2) f_j^n + \beta^3(\alpha + 3\alpha^2)\Delta x \partial_x f_j^n \\ & + 0.5\beta^3\alpha^2\Delta x^2 \partial_x \partial_x f_j^n + \alpha^3(1 + 3\beta + 6\beta^2) f_{j+1}^n \\ & - \alpha^3(\beta + 3\beta^2)\Delta x \partial_x f_{j+1}^n + 0.5\alpha^3\beta^2\Delta x^2 \partial_x \partial_x f_{j+1}^n, \end{aligned} \tag{7}$$

where $\alpha = (X - x_j)/\Delta x$ and $\beta = (x_{j+1} - X)/\Delta x$ with the departure point X located between x_j and x_{j+1}. The notations $x_j = j\Delta x$, $t^n = n\Delta t$, and $f_j^n = f(t^n, x_j)$ are used for simplicity. QI2 only requires the same reference points as those required in CHI when the derivatives are approximated by fourth-order central finite difference methods. Note that CHI and QI2 conserve mass, while CLI does not. All interpolations above do not satisfy the conservation of the L2 norm and the positivity of f: the latter is not required for δf gyrokinetic simulations.

4. Numerical Results

4.1 Linear advection

First, let us consider the one-dimensional advection problem with constant velocity u:

$$\frac{\partial y}{\partial t} + u\frac{\partial y}{\partial x} = 0, \tag{8}$$

where $0 \le x \le L$ and $y(t, 0) = y(t, L)$. The analytical solution $y(t, x) = y(0, x - ut)$ is not exactly satisfied in numerical simulations because of numerical dissipation and dispersion. To evaluate the numerical errors, one can analyze schemes using the Fourier expansion

$$y_i^n = \sum_{j=0}^{N-1} \hat{y}^n(k_j) \exp(ik_j x_i), \tag{9}$$

where N and $k_j = 2\pi j/L$ are the number of grid points and wave number, respectively. Following Imai [8], the gain error G_E and the phase error Θ_E for each wave number are calculated as

$$G_\mathrm{E}(k_j) = 1 - \left|\frac{\hat{y}^n(k_j)}{\hat{y}^0(k_j)}\right|^{\frac{1}{k_j|u|t^n}}, \tag{10}$$

$$\Theta_\mathrm{E}(k_j) = \left|1 - \frac{1}{k_j|u|t^n} \arg\left(\frac{\hat{y}^n(k_j)}{\hat{y}^0(k_j)}\right)\right|, \tag{11}$$

respectively. The gain and phase errors are plotted in Fig. 1 as a function of the wave number. For reference, the results of two Eulerian schemes are also plotted, where the third-order upwind (UF3) and the fourth-order central finite (CF4) differences are implemented with the fourth-order Runge-Kutta-Gill (RKG) method for time integration. Figure 1 (a) shows that the gains of CLI and CHI are accurate to third order, while the gain of QI2 is accurate to fifth order in $G_{\rm E}$. The results of CHI and QI2 are less dissipative than that of UF3. While the central finite difference method itself does not cause numerical dissipation,

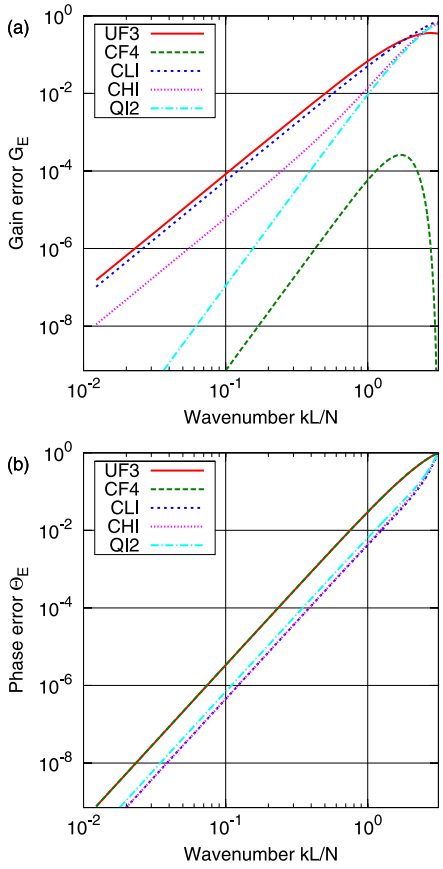

Fig. 1 (a) Gain errors $G_{\rm E}$ and (b) phase errors $\Theta_{\rm E}$ as a function of the wave number k (where $L = 2\pi$, $N = 512$, and $C = 0.4$). The results of three interpolation schemes (CLI, CHI, and QI2) and two Eulerian schemes (UF3 and CF4) are plotted.

CF4 has the smallest dissipation due to time integration by the RKG method. All schemes have fourth-order accuracy for the phase, as shown in Fig. 1 (b).

Note that the errors in semi-Lagrangian schemes periodically depend on the Courant number $C = |u|\Delta t N/L$, while the errors in explicit Eulerian schemes monotonically grow as $C \to 1$. The error dependence on the Courant number is similar to that obtained by Filbet [9].

4.2 Dynamics in parallel phase space

Results of benchmark tests for trapped and passing particle motions are demonstrated in this section. Equation (2) expresses that the parallel dynamics is regarded as an advection of a distribution function along equi-contour lines of the particle kinetic energy K in the phase space $(z, v_\parallel)$ [see Fig. 2 (a)]. The contours with $K < \mu B_0/m_{\rm i}$ correspond to trapped particle trajectories, and the others represent trajectories of passing particles. There is a separatrix with an X-point because the magnetic field strength is given by $B/B_0 = 1 - \epsilon\cos z$, where B_0 and ϵ are the magnetic field strength on the magnetic axis and the inverse aspect ratio, respectively.

The time integration of Eq. (2) is computed by using the second-order splitting method and CHI. The initial profile is given by $f(z, v_\parallel, t = 0) = F_{\rm M}(K)\exp\left[-(z/0.2\pi)^2\right]$, where $-\pi \le z \le \pi$ and $-5 \le v_\parallel/v_{\rm thi} \le 5$. The ion thermal velocity is denoted by $v_{\rm thi}$. We employ 256×256 grid points to discretize the parallel phase space and a time step size of $\Delta t/t_{\rm tr} = 0.032$, where $t_{\rm tr} = qR_0/v_{\rm thi}$. The periodic and zero-fixed boundary conditions are assumed in the z and $v_\parallel$ directions, respectively. Snapshots of equi-contours of the distribution function are shown in Fig. 2 (b)-(d). The distribution function is advected along the contour lines of the particle kinetic energy (see also Fig. 2 (a)). The ballistic motion of passing particles elongates the profile and makes fine-scale structures. When the scale length of the fine structures reaches the grid size, unphysical fluctuations may appear. Physically, a dissipation mechanism (e.g., collisions in velocity space) is required to stabilize the high-wave number modes, where we have to employ sufficient number of grid points to represent the typical scale length of the dissipation. Similar requirements are found in flux tube gyrokinetic simulations with non-periodic boundary conditions along the field lines for

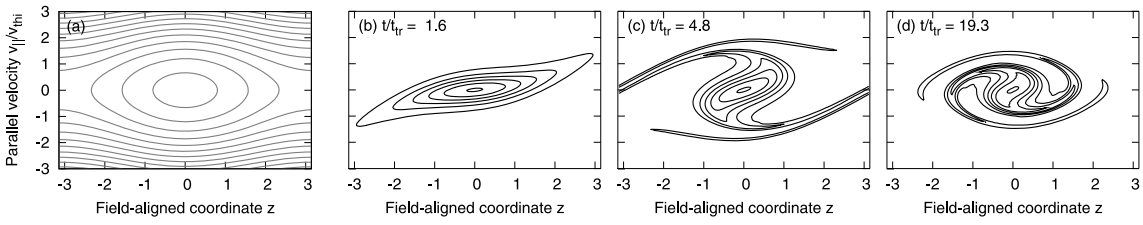

Fig. 2 (a) Contour lines of the particle kinetic energy K, and (b)-(d) snapshots of equi-contours of the distribution function f in parallel phase space (where $\epsilon = 0.18$ and $\mu B_0/T_{\rm i} = 4.0$). Horizontal and vertical axes are defined by z and $v_\parallel$, respectively.

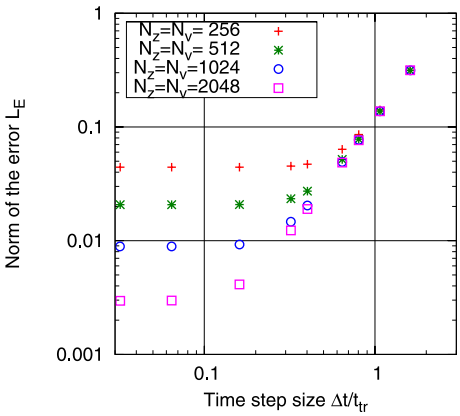

Fig. 3 Norms of the errors L_E at $t/t_{tr} = 3.2$ as a function of the time step size Δt for several N_z and N_v. Minimum period of the particle passing motions is $T_{min} = qR_0 2\pi/v_{\parallel,max} = 1.25t_{tr}$, where $v_{\parallel,max}/v_{thi} = 5$.

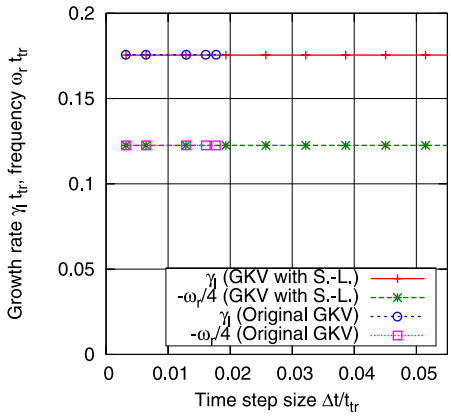

Fig. 4 Linear growth rates γ_l and real frequencies ω_r as a function of the time step size Δt (where $k_y\rho_i = 0.14$ and $N_z = 64$). Results using the semi-Lagrangian scheme for the parallel dynamics are compared with the original GKV results.

$k_y \neq 0$ and $\hat{s} \neq 0$ (where k_y and $\hat{s}$ are the poloidal wave number and magnetic shear, respectively), because the distribution function is also elongated by sheared Hamiltonian flows in toroidal configurations. Instead of physical dissipation, in this paper, numerical dissipation contributes to stabilization.

To estimate the temporal accuracy of the present method, we evaluate the norm of the errors L_E defined by

$$L_E = \sqrt{\sum_{i=1}^{N_z}\sum_{j=1}^{N_v}\left|f_{i,j} - f_{i,j}^{ref}\right|^2 \Big/ \sum_{i=1}^{N_z}\sum_{j=1}^{N_v}\left|f_{i,j}^{ref}\right|^2}, \qquad (12)$$

where N_z and N_v are the number of grid points in the z and $v_\parallel$ coordinates, respectively. The reference solution $f_{i,j}^{ref}$ is computed with finer spatial mesh sizes ($N_z = N_v = 4096$) and a smaller time step size ($\Delta t/t_{tr} = 0.0032$). Figure 3 plots L_E as a function of the time step size. The second-order temporal accuracy of the scheme is confirmed in the range of $\Delta t/t_{tr} \geq 0.2$, as expected. For smaller Δt, however, there is a plateau regime where spatial errors dominate [10]. Because the spatial errors are dominant for practical parameters, we can obtain sufficiently accurate results for larger time steps than those restricted by the CFL condition, e.g., $\Delta t < qR_0 2\pi/v_{\parallel,max}N_z = 0.0049t_{tr}$ for $v_{\parallel,max}/v_{thi} = 5$ and $N_z = 256$. It is encouraged to use semi-Lagrangian schemes because Eulerian schemes require a significantly smaller time step size. The present result demonstrates that the semi-Lagrangian scheme allows us to take a time step size sixty times larger than that restricted by the CFL condition, with desirable temporal accuracy.

4.3 Ion temperature gradient instability

Tests of a gyrokinetic simulation of the linear ITG instability are carried out for the Cyclone DIII-D base case parameter set [11]. The time integration of Eq. (1) is split into two parts: one with the the parallel motions (Eq. (2)) and one without them. The former is computed by using CHI (QI2 gives the same results), and the latter is computed by using the RKG method. Figure 4 plots the linear growth rate and real frequency as a function of the time step size for a low-k_y mode, where the CFL restriction due to the parallel motions is more severe than that due to the perpendicular drift motions in the original Eulerian GKV code. The results agree well with those obtained by the original GKV code: their relative errors are less than 0.1%. Therefore, the new solver with the semi-Lagrangian scheme enables us to take larger time step sizes than that in the CFL condition of $\Delta t/t_{tr} \sim 0.02$ and still achieve accurate results. The maximum time step is controlled not by the parallel motions but by the perpendicular drift motions, and is estimated as $1/v_{d,max}k_\perp \sim 0.055t_{tr}$ with the parameters for the case in Fig. 4.

5. Summary

We made the first application of a semi-Lagrangian scheme to a flux tube gyrokinetic simulation in three steps: linear advection, trapped and passing particle motions, and linear ITG instability in a flux tube geometry. First, the spatial accuracy of the schemes was evaluated for the linear advection problem. CHI and QI2 schemes were less dissipative than the UF3 scheme and less dispersive than the UF3 and CF4 schemes. Second, a study of the accuracy of the parallel dynamics revealed that spatial errors dominated rather than temporal ones, because the sheared flow pattern in the phase space elongated the profile of the distribution function and generated fine-scale structures. The result demonstrated that a semi-Lagrangian scheme is advantageous to simulate the parallel dynamics, because it allows us to increase the time step size without the CFL restriction. Finally, applying the semi-Lagrangian scheme to the parallel dynamics enabled us to take larger time step sizes in simulations of a low-k_y mode of the linear ITG in-

stability. Semi-Lagrangian schemes should be more useful for flux tube simulations including both kinetic ions and electrons, because the electron thermal speed is faster than that of ions by the square-root of the mass ratio for $T_e = T_i$. Our near-term future work will extend the GKV code to deal with electron dynamics.

[1] M. J. Pueschel, T. Dannert and F. Jenko, Comput. Phys. Commun. **181**, 1428 (2010).
[2] V. Grandgirard *et al.*, Plasma Phys. Control. Fusion **49**, B173 (2007).
[3] T.-H. Watanabe and H. Sugama, Nucl. Fusion **46**, 24 (2006).
[4] M. A. Beer, S. C. Cowley and G. W. Hammett, Phys. Plasmas **2**, 2687 (1995).
[5] H. Yoshida, Phys. Lett. A **150**, 262 (1990).
[6] T.-H. Watanabe and H. Sugama, Trans. Theory Stat. Phys. **34**, 287 (2005).
[7] G. Farin, *Curves and Surfaces for CAGD: A Practical Guide* (Morgan Kaufmann, San Francisco, 2002) p. 106.
[8] Y. Imai and T. Aoki, J. Comp. Phys. **217**, 453 (2006).
[9] F. Filbet and E. Sonnendrücker, Comput. Phys. Commun. **150**, 247 (2003).
[10] C. C. Ober and J. N. Shadid, J. Comput. Phys. **195**, 743 (2004).
[11] A. M. Dimits *et al.*, Phys. Plasmas **7**, 969 (2000).